Effects of Cover Sheets on the Nugget Growth and Fracture Behavior of Resistance Spot Welded Q&P980 Steel Joints

Zhanxiang Ling, Ting Chen, Liang Kong[*] and Min Wang[*]

Abstract

The resistance spot weldability of galvanized ultra-high-strength steels is not satisfied, the joints are prone to interfacial fracture and the weldable current range is narrow. To solve the problems, a novel method called resistance spot welding with double-sided cover sheets was introduced to weld a galvanized Q&P980 steel with the thickness of 1.2 mm. Two thin SPCC mild steel sheets were chosen as cover sheets and were placed symmetrically at both sides between the Q&P980 steels and the electrodes, then the RSW process was carried out. Compared with the traditional RSW method, the joints obtained by using the novel method achieved larger tensile shear strength and energy absorption, which increased by 26.9% and 52.6%, respectively. With increasing the welding current, the failure mode transferred from interfacial fracture to nugget pull-out fracture or base metal tearing fracture. By contrast, the joints always showed interfacial fracture without cover sheets. The improvement of the joint performance was mainly attributed to the enlargement of the nugget. With the help of finite element simulation, it was found that the cover sheets helped increase the contact area and reduced the current density during welding, which postponed the expulsion, and a larger area could be evenly heated. The application of the novel method can be easily extended to the resistance spot welding of other ultra-high-strength steels with various thicknesses.

Keywords: Resistance spot welding, Q&P980 steel, Cover sheet, Mechanical property

1 Introduction

Owing to the urgent need to reduce weight of cars in automobile industry, ultra-high-strength steels (UHSSs) are increasingly used in body-in-white to replace traditional low carbon steels due to their superior strength-to-weight ratios. These steels are always coated by zinc to improve corrosion resistance. Resistance spot welding (RSW) is a commonly used joining method for structural components during body-in-white fabrication. Thus, the feasibility to join galvanized UHSSs by RSW determines whether they can be successfully introduced to automobile manufacturing. However, the resistance spot weldability of galvanized UHSSs is not satisfied. Pouranvari and Marashi [1] pointed out the RSW joints of UHSSs exhibited early expulsion and a higher tendency to fail in interfacial fracture (IF) mode. It is an undesired fracture mode from the viewpoint of product liability law. The existence of zinc coating further worsens the weldability of UHSSs. For example, Ji et al. [2] found that there was no weldable current range for the zinc-coated hot-stamped boron steel, but a 2 kA weldable current range was observed for the aluminum-silicon-coated hot-stamped boron steel.

To solve the problems and improve the weldability of UHSSs, many methods have been introduced, and they can be classified into several categories. The first one is to adjust the welding parameters. Tumurulu [3] suggested that increasing electrode force could widen the weldable current range for DP780 steel, as well as increase the nugget diameter. Zhao et al. [4] found that tensile shear strength of DP600 steel under electrode force of 3.5 kN

*Correspondence: ingerkongliang@sjtu.edu.cn; wang-ellen@sjtu.edu.cn

Shanghai Key Laboratory of Materials Laser Processing and Modification, Shanghai Jiao Tong University, Shanghai 200240, China

Ling *et al. Chinese Journal of Mechanical Engineering*   (2022) 35:96

Page 2 of 14

is larger than that under 2.0 kN, 2.5 kN and 4.0 kN. Cretteur et al. [5] found that using the in-situ heat treatment, i.e., pre-heating and post-heating during RSW could help eliminate cracks at the interface edge, thereby improved the joint quality. Pouranvari [6] pointed out that postweld in situ tempering increased the properties of martensitic stainless-steel joints but worsened the DP600 steel joints. Chabok et al. [7], Eftekharimilani et al. [8] and Liu et al. [9] all used a double pulse schedule to weld UHSSs, and observed quality improvement of the resistance spot welded joints compared with the single pulse weld schedule. Chen et al. proposed a stepped current pulse schedule to improve the weldability of a press hardened steel and found the schedule helps inhibit expulsion, increase nugget size and decrease the notch root stress concentration [10]. Although these methods are valid more or less, it is limited to improve the weldability of UHSSs via simply changing welding parameters. The second one is to modify the welding equipment. Yu et al. [11] introduced the medium frequency direct current (MFDC) constant power control (CPC) welding machine to improve the weldability of 1 GPa grade TWIP steel, they found that compared with MFDC constant current control (CCC) welding machine, CPC could help reduce expulsion at the early stage of the welding process, and then higher heat input could be applied to the welding area. As a result, larger nugget size and higher tensile shear strength were obtained in CPC welding than CCC welding. Li et al. [12] installed two permanent magnets on both electrodes, the generating external magnetic field could stir the weld pool during RSW and elongated the nugget. Thus, the joint strength was improved. The third one is to modify the microstructure of the nugget by introducing an interlayer. Aghajani and Pouranvari [13] introduced a nickel interlayer to weld martensitic stainless steel, the interlayer altered the nugget microstructure from dual phase microstructure of martensite and δ-ferrite to austenitic microstructure, which helped the joints achieve pull-out fracture mode and higher energy absorption. The last one is to introduce a cover sheet between the electrode and the sheet to be welded, the method was frequently applied to weld nonferrous metals such as Mg [14], or dissimilar RSW such as Al/steel [15], but was hardly reported in the RSW of steels. Yu [16] introduced a CrNi cover sheet when resistance spot welding SGACEN/DP980/CP1180 three-steel sheets,

the cover sheet was placed at one side between SGACEN steel and the electrode, they found that the nugget could grow to the SGACEN/DP980 interface after using the cover sheet. Owing to the shift of the nugget, the tensile shear strength of that interface was increased and the suitable welding range was expanded.

Nugget size is the most important parameter governing the mechanical performance of the spot welds [17]. The critical nugget diameter to avoid interfacial fracture for UHSSs is always large, but the early expulsion restrains the increase of nugget diameter. To postpone the expulsion and increase the nugget size, a method called RSW with double-sided cover sheets was proposed to weld a 3rd generation UHSS, galvanized Q&P980 steel. A thin cold-rolled SPCC low carbon steel was chosen as the cover sheet. RSW without cover sheets was also conducted for comparison. The tests and observations on microstructure, mechanical performance, nugget formation process and fracture behavior were carried out to illuminate the influence of cover sheets on the weldability of the Q&P980 steels, finite element simulation of the RSW process was conducted to explain some of the experiment results.

2 Experimental
2.1 Materials
1.2 mm-thick galvanized Q&P980 steels with a coating thickness of 10 μm were used as the base metals. For the sake of low cost and availability, uncoated cold-rolled SPCC mild steel sheets with a thickness of 0.2 and 0.3 mm were used as the cover sheets. The chemical compositions of the materials are listed in Table 1.

2.2 Welding Process
The experimental setup of RSW with double-sided cover sheets is shown in Figure 1a. The cover sheets were placed between electrodes and Q&P980 steel sheets symmetrically at both side, welding process was then carried out at the position of cover sheets using a medium frequency direct current (MFDC) RSW machine. Figure 1b shows the configuration of the welding joints subjected to tensile shear tests; the dimensions of sheets are in accordance with the ISO18272-2 standard. Six joints were welded for each welding parameter, three for tensile shear test and three for cross-sectional examination. For comparison, joints without cover sheets were also

Table 1 Chemical composition of Q&P980 and SPCC steel (mass fraction, %)

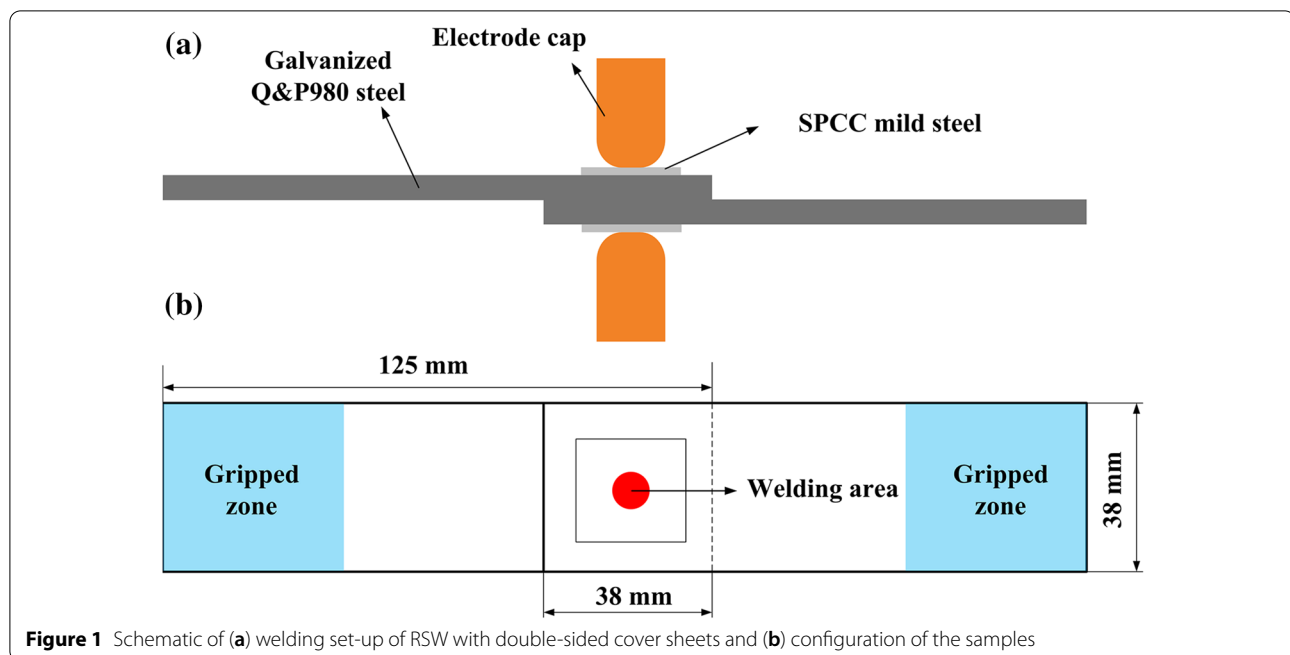| Material	Mn	Si	C	Al	S	P	Fe
Q&P980	2.248	1.774	0.1792	0.0418	0.0002	0.0075	Bal.
SPCC	0.024	–	0.045	0.034	0.01	0.01	Bal.

Figure 1 Schematic of (**a**) welding set-up of RSW with double-sided cover sheets and (**b**) configuration of the samples

Table 2 Specific welding parameters used in the experiment

Welding parameter	Experimental condition
Number of welding pulses	3
Cooling time between pulses	20 ms
Welding time per pulse	120 ms
Electrode force	4.5 kN
Holding time	250 ms
Welding current	5.5 kA - expulsion (0.5 kA interval)

prepared. A triple-pulse welding schedule was selected, and the specific welding parameters are shown in Table 2. The electrode cap is the Cu-Cr-Zr dome-radius type with a tip diameter of 6 mm.

2.3 Post-weld Test
After welding, tensile shear tests were performed using a universal materials tester at 1 mm/min to obtain tensile shear curves. Peak loads and energy absorptions at the peak load were then extracted from these curves. The rest joints were cut using a wire cutting machine to obtain joint cross-sections. Following standard metallographic procedures, a 3% nital solution was used to etch the samples for 3 s for microstructure observation, and a saturated picric acid solution was also used to etch the samples in 30 °C water bath for 2 min to more clearly reveal the nuggets. The joint profiles were studied using a ZEISS stemi 305 stereomicroscope and ZEISS AX10 optical microscope (OM). The microstructures

and fracture morphologies were observed via a VEGA-3-XMU scanning electron microscope (SEM) equipped with an AZtec X-MaxN80 energy dispersive spectrometer (EDS). Microhardness was measured using a Zwick/Roell ST-2000 micro-Vickers hardness tester with a load of 500 g and a holding time of 15 s.

2.4 Finite Element Method (FEM) Simulation
A two-dimensional axisymmetric finite element model was created in ANSYS 17.2. The model involves the solution of mechanical, thermal and electrical fields and the sequential coupling of these fields. The simulation method was similar with the work of Wan et al. [18] on the numerical simulation of the Al/steel RSW process, which was developed by our group, detailed description of the model can be found in that work.

3 Results and Discussion
3.1 Microstructure
For each experimental set-up, i.e., without cover sheets, with 0.2 mm cover sheets and with 0.3 mm cover sheets, the specimen under the critical current was selected to reveal its microstructure, as shown in Figure 2. The critical current represents the highest current at which no expulsion occurs in the experiment. Figure 2a–c shows the cross-sectional view of the joints for different set-ups. After using cover plates, the critical current increases and the enlargement of the nugget diameter and penetration depth can be clearly seen. When 0.2 mm cover plates were used, the cover plates
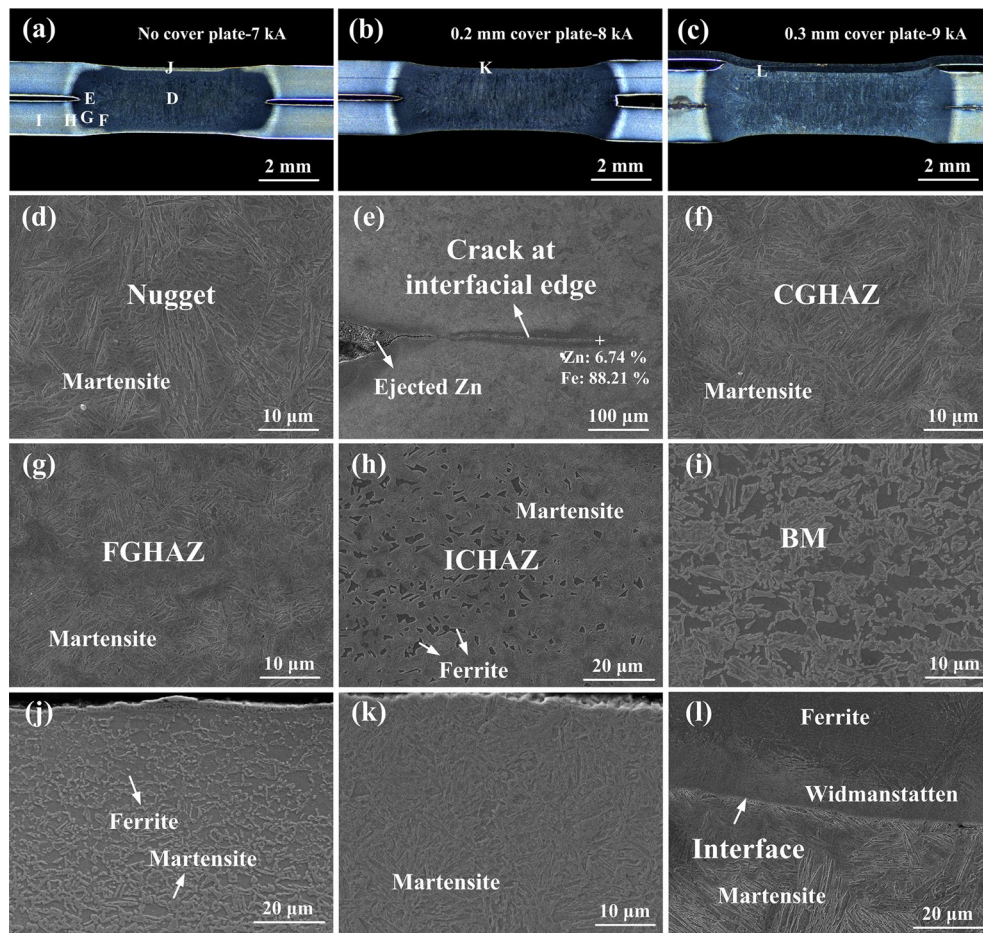
Figure 2 Cross-sectional view of joints (**a**) without cover sheets; (**b**) with 0.2 mm cover sheets and (**c**) with 0.3 mm cover sheet under critical welding current and (**d–j**) microstructure corresponding to the locations D-J in **a**; **k**, **l** microstructure corresponding to the locations K in **b** and L in **c**

would not be welded to the Q&P steel, it is a desired result as there is no additional weight for the joint, which makes the method feasible in industry. However, the 0.3 mm cover plate at positive electrode side was welded to the Q&P steel under critical welding current. According to Zhou et al., owing to the Peltier and Thomson effect [19], more heat was accumulated at the positive electrode side for the MFDC welder. Thus, the cover sheet at positive side was more prone to be welded to the Q&P steel. In the experiment, the 0.3 mm cover sheets couldn't be easily removed once the current reached 8 kA, making it less feasible. Microstructures of region D-L marked in Figure 2a–c are shown in Figure 2d–l, respectively. Region D is the nugget formed at the interface of Q&P980 steels, it consists of coarse lamellar martensite because the high carbon equivalent of the base metal and high cooling rate during RSW process. Region E is the interfacial edge, corona bond is formed here during welding to prevent expulsion.

A crack can be seen and it extends to the edge of the nugget. EDS analysis at the crack indicates that the Zn content is abnormally high, the result suggests that the Fe-Zn reaction products exist inside the crack. It can be deduced that the formation of these products is owing to the incomplete ejection of the zinc coating at the interfacial edge during welding, and impedes the effective bonding here. Region F is the coarse-grain heat affect zone (CGHAZ), the CGHAZ is adjacent to the nugget, the temperature here was far beyond Ac3, sufficient time and temperature was supplied for the austenite grains to grow, and it transformed to the coarse martensite after welding. Region G is the fine-grain heat affect zone (FGHAZ), the FGHAZ is away from the nugget, the temperature here was slightly beyond Ac3, thus there was no sufficient time for the austenite grains to grow, and it transformed to the fine martensite after welding. Region H is the inter-critical heat affect zone (ICHAZ), the temperature here was between Ac3

Ling *et al. Chinese Journal of Mechanical Engineering*   (2022) 35:96

Page 5 of 14

and Ac1, thus partial austenization occurred, the austenitized part transformed into martensite after welding, and the rest part remained untransformed. Thus, the ferrite in the base metal sporadically distributed at ICHAZ, as shown in Figure 2h. Region I is the base metal, and it consists of martensite, ferrite and retained austenite. The corresponding regions for the other two joints are rather similar, so the micrographs were not included in the figure. However, the microstructure at the surface of the Q&P steel differs for different set-ups. When no cover plate was used, the surface of the Q&P steel, region J, was directly contacted with the electrode, and was severely cooled by it, thus no phase transition happened here and the microstructure is the tempered structure of base metal. As shown in Figure 2j, the content of martensite reduces compared with the base metal. However, when cover plates were used, the Q&P steel was replaced by the cover plate to bear the cooling effect of the electrode, which made the temperature at the surface of the Q&P steel exceed Ac3, Region K and region L shows martensite structure, which proves that fully austenization happened here. Besides, although the 0.3 mm cover plate was welded to the Q&P steel, a clearly interface is shown in Figure 2l, it indicates that no nugget was formed between the cover plate and Q&P steel.

3.2 Mechanical Performance

Pouranvari and Marashi [20] reported that RSW joints had a greater tendency to fail in the IF mode under tensile shear loading than cross-tension loading or coach peel loading conditions. Thus, the tensile shear test was carried out in the experiment as the avoidance of IF mode would guarantee its avoidance in other loading conditions.

Tensile shear curves of different joint set-ups under critical welding current are shown in Figure 3, and the inserted pictures show the corresponding fracture modes. Without cover sheets, the joint shows IF mode and it has the smallest peak load and displacement, the curve shows a sudden decline once reaching the peak load. With 0.2 mm cover sheets, the joint shows base metal tearing fracture (TF). Fracture initiated at the edge of the weld spot and propagated to the base metal, which was then torn up from the edge of the weld spot to the side. The curve shows a gradual decline after the tearing of the base metal, so a large displacement is obtained. Similar fracture mode was reported by Alizadeh-Sh et al. [21] when resistance spot welding a ferrite stainless steel. With 0.3 mm cover sheets, a common nugget pull-out fracture (PF) occurred, the nugget was quickly pulled out from one of the sheets during fracture, so the curve descends rapidly after reaching the peak load. In general,
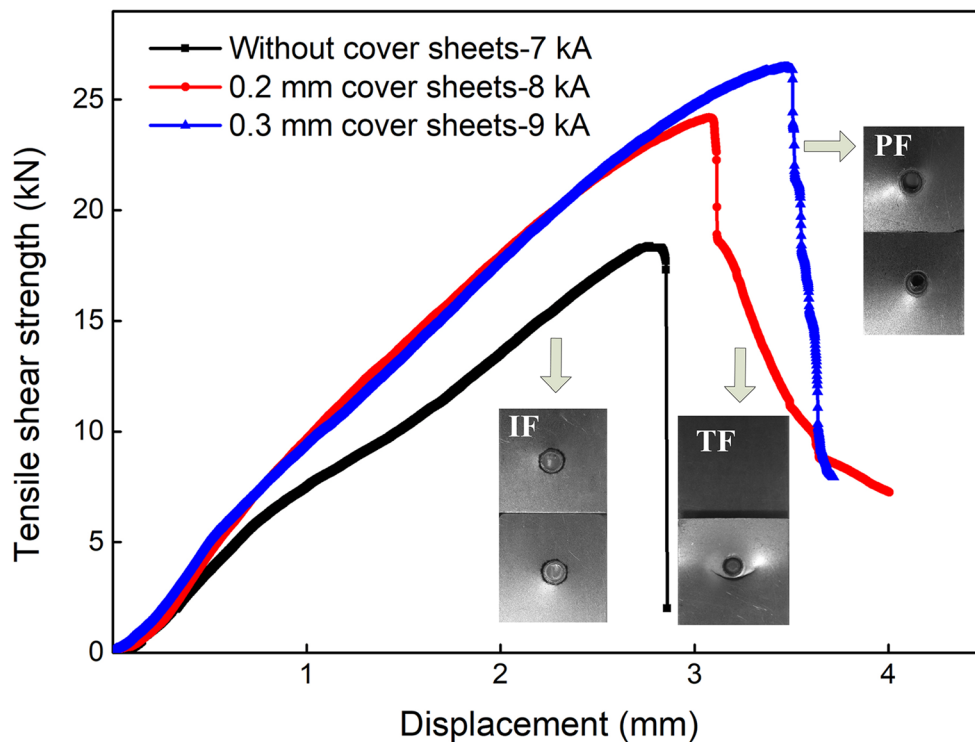

Figure 3 Typical tensile shear curves of joints with and without cover sheets under critical welding current

Ling *et al. Chinese Journal of Mechanical Engineering*   (2022) 35:96

Page 6 of 14

the joints owned better performance after using the cover sheets.

To comprehensively understand the effect of the cover sheets on the mechanical properties of the RSW joints, nugget diameter and penetration depth of each joint were measured, and peak load and energy absorption of each joint were extracted from their tensile shear curves. The results are shown in Figure 4. Generally, the nugget diameter increases with increasing the welding current until expulsion for all set-ups, the nugget penetration depth, tensile shear strength and energy absorption show similar variation tendency with the nugget diameter. Expulsion occurred under welding current of 7.5 kA, 8.5 kA, 9.5 kA without cover sheets, with 0.2 mm cover sheets and with 0.3 mm cover sheets, respectively. Obviously, the cover sheet can help postpone the expulsion. The nugget diameter severely reduced under the expulsion current, so did the peak load and energy absorption. The results differ from the work of Pouranvari et al. [22] on the RSW of low carbon steels, only energy absorption was reduced for the expulsion samples according to their results. All joints showed IF mode without cover sheets.

However, with 0.2 mm cover sheets, the joints showed IF mode under current below 7.5 kA, and then transformed to TF mode. With 0.3 mm cover sheets, the joints showed IF mode under current below 8.5 kA, and then transformed to PF mode. Although expulsion occurred under higher current with 0.3 mm cover sheets, and the achievable joint strength was higher than that with 0.2 mm cover sheets, the cover sheets would be welded to the Q&P steel when welding current exceeded 8.0 kA, so the 0.2 mm cover sheets should be more suitable for industrial application as they wouldn't be welded to the Q&P steels under all welding current. The achievable nugget diameter, nugget penetration depth, tensile shear strength and energy absorption increase by 18.5%, 13.8%, 26.9% and 52.6%, respectively for joints with 0.2 mm cover sheets compared with that without cover sheets. The improvement of mechanical performance should be mainly attributed to the increase in nugget size. From Figure 4a, it can also be concluded that the commonly referred critical nugget diameter criterion, $4\sqrt{t}$, which is suggested by AWS D8.9 standard, and $5\sqrt{t}$, which is suggested by JIS Z3140 standard and DVS 2923 standard,
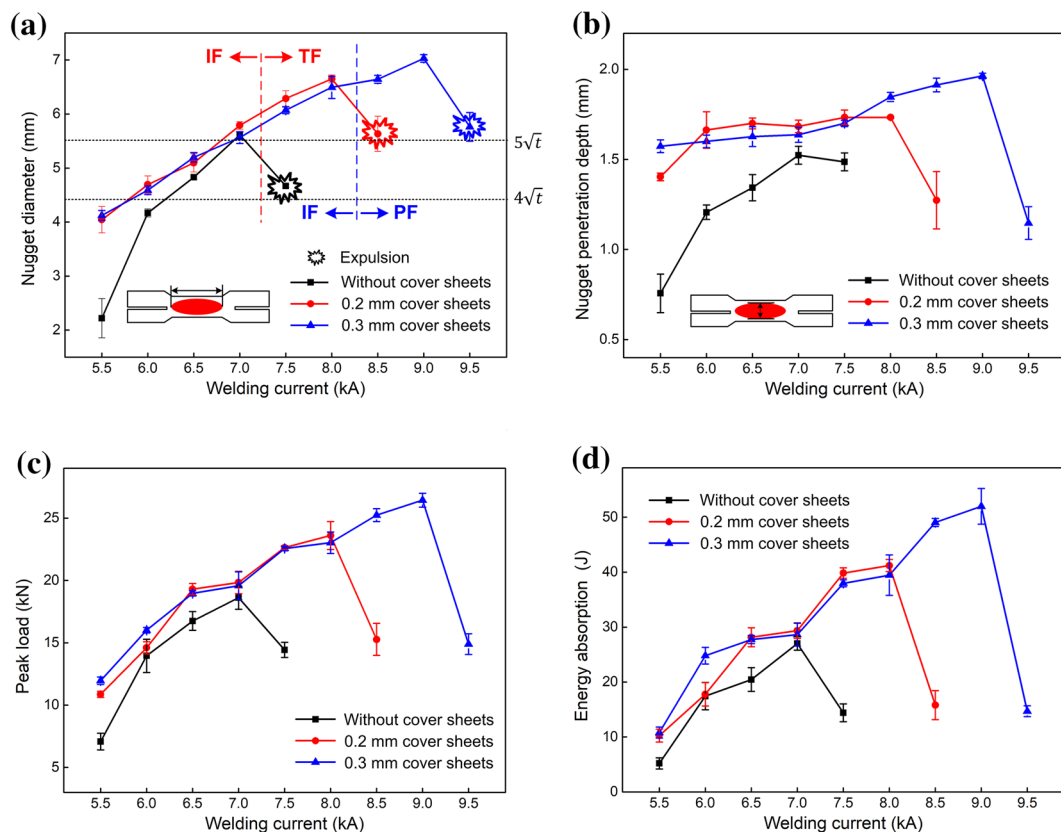

Figure 4 Line graphs of (**a**) nugget diameter, (**b**) nugget penetration depth, (**c**) tensile shear strength and (**d**) energy absorption as a function of welding current for different joint set-ups

can no longer guarantee the avoidance of IF mode. Thus, a modified criterion should be established for the RSW of UHSSs in the future.

Figure 5 demonstrates the microhardness distributions of different joint set-ups under critical welding current. The hardness values are directly linked to the microstructures. The high hardness of nugget is attributed to the formation of lath martensite, so as the CGHAZ. The hardness of FGHAZ is highest owing to the fine grain size of martensite. Hardness value changes sharply at the ICHAZ. A slight hardness decrease exists between the ICHAZ and base metal, this region is defined as a subcritical heat affect zone (SCHAZ). Softening at SCHAZ was frequently reported in the RSW of martensite-containing UHSSs, and the phenomenon was due to the tempering of martensite at this region as claimed by Tamizi et al. [23]. Spena et al. [24] also observed a hardness decrease of about 40 HV in the softening region of Q&P steel. The overall hardness distributions are similar for different set-ups, except that the hardness of nugget and HAZ in the joint with cover sheets is slightly lower than that without cover sheets. As the microstructures are similar, we try to explain the difference of hardness by comparing the cooling rates. Temperature histories of different regions obtained from FEM simulation results are shown in Figure 6. During welding, as the Q&P steels

with cover sheets were not directly cooled by the electrode, the cooling rate of the welding zone was lower compared with that without cover sheets, which can be seen from the slope of the curves. According to Sirin et al. [25], the most critical cooling range was between 800 °C and 500 °C, which was defined with the value $t_{8/5}$, namely cooling time between 800 °C and 500 °C. With 0.2 mm cover sheets, $t_{8/5}$ at nugget and HAZ is about four times compared with that without cover sheets. The lower cooling rate helps reduce the hardness of nugget and HAZ, and the low hardness is beneficial to the overall toughness of the weld spot.

3.3 Nugget Growth

From the above results, it can be concluded that the improvement of the mechanical properties of RSW joints after using cover sheets is mainly attributed to the increase of nugget size. To understand the difference between the nugget growth with and without cover sheets, RSW was carried out and interrupted at a specific time to obtain the characteristic of nugget at different time, the results are shown in Figure 7. Without cover sheets, a high temperature HAZ was firstly formed at the interface of the two sheets. However, with cover sheets, the HAZ was firstly formed inside the Q&P steels. Obviously, the cover sheets modified the heat distribution at
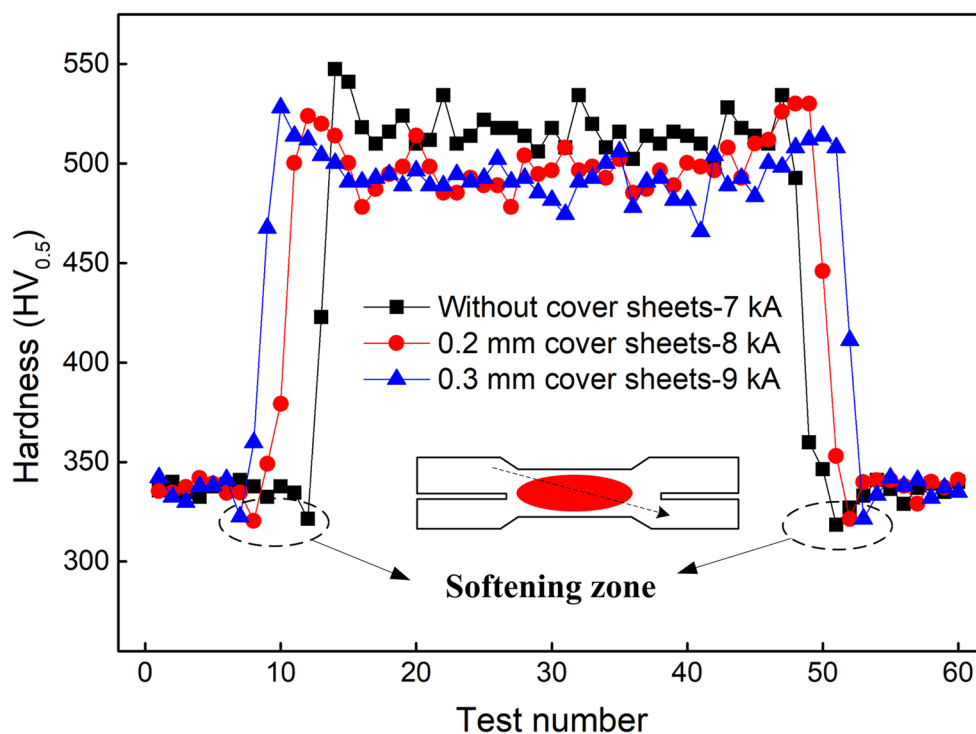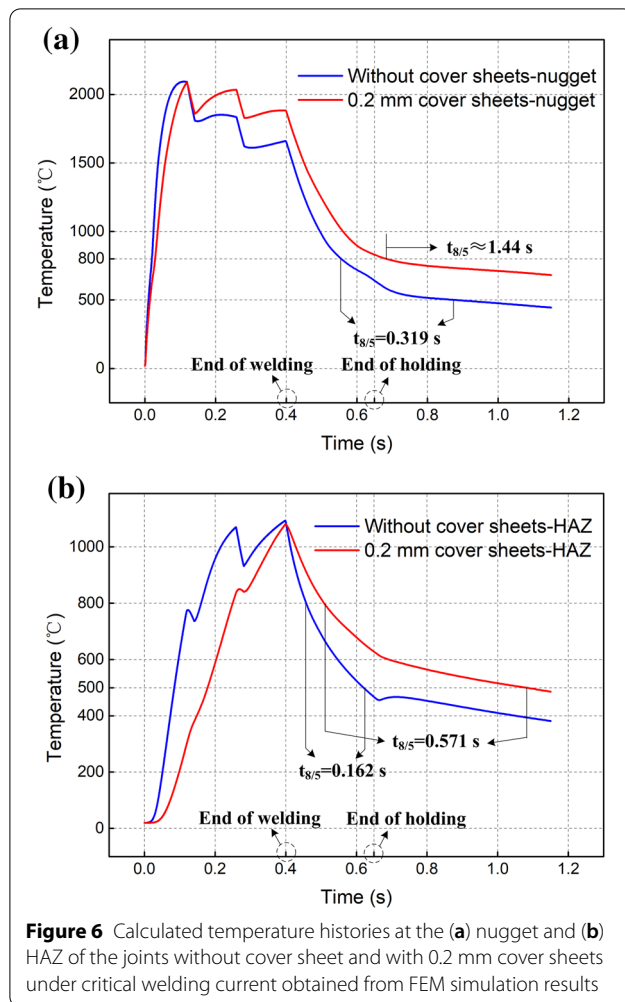

Figure 5 Hardness distributions of joints with and without cover sheets under critical welding current

Ling *et al. Chinese Journal of Mechanical Engineering*   (2022) 35:96

Page 8 of 14

Figure 6 Calculated temperature histories at the (**a**) nugget and (**b**) HAZ of the joints without cover sheet and with 0.2 mm cover sheets under critical welding current obtained from FEM simulation results

the beginning of welding, the contact resistance between the cover sheets and Q&P steels caused the shift of the high temperature HAZ. The nugget then formed at the interface of Q&P steels and continued to grow. Under 7 kA, the growth of the nugget was faster without cover sheets than with cover sheets. However, the nugget size stabilized during the third pulse without cover sheets. In contrast, the nugget continued to grow during the third pulse with 0.2 mm cover sheets. Eventually, the nugget diameters of the two joints were similar. The excessive nugget growing rate at the beginning of welding is one of the reasons that expulsion occurs under low welding current without cover sheets. With cover sheets, RSW could be carried out under higher welding current (8 kA) without expulsion, and the nugget could fully grow during the entire welding period, resulting in a larger nugget. The primary, secondary and tertiary nugget caused by the pulse current can be clearly distinguished in the joint without cover sheets, but they are not obvious in the joints with cover sheets. It is due to the cover sheets

interfered the cooling between the electrode and the sheet, and the majority of the nugget remained molten during the cooling time between welding pulses.

The larger achievable nugget size after using cover sheets can be explained by the current density distributions obtained from the FEM simulation results, as shown in Figure 8. During welding, current flowed from the upper electrode to the lower electrode, and the current gathered at the edge of the contact surface, resulting in the largest current density here among the surface. At the beginning of RSW, the contact areas at the surface and interface of the Q&P steel were similar, but with the progress of welding, the contact areas at the surface and interface became larger with cover sheets than that without cover sheets. It is because that the cover sheet was softer than the Q&P steel, the electrode could press faster into the cover sheet during welding, resulting in a rapid increase of contact area between them. The electrode force was transmitted by the cover sheet to the Q&P steel, owing to the large contact area between the electrode and the cover sheet, the contact areas at the surface and interface of the Q&P steel were always larger compared with the joint without cover sheets during welding. The larger contact area offered a larger passageway for the current to flow and reduced the current density. As a result, under critical welding current, the current density was similar with cover sheets compared with that without cover sheets during RSW, regardless the welding current was higher with cover sheets. Consequently, a larger area was evenly heated during welding, which explained the postpone of expulsion and the increase of the nugget diameter. Besides, owing to the heat generation of contact resistance between the cover sheets and the Q&P steels and the Q&P steels were away from the water-cooling electrode, the penetration depth of the nugget also became larger.

3.4 Failure Analysis

As mentioned above, the joints for different set-ups demonstrate different fracture modes. The typical fracture modes without cover sheets, with 0.3 mm cover sheets and with 0.2 mm cover sheets are IF, PF and TF, respectively. The cross-sectional view of the typical fractured joints and the detailed pictures of the fractured positions are shown in Figure 9. To reveal the underlying reasons for different fracture modes, schematics of failure mechanisms for different failure modes are shown in Figure 10, in which red ellipses represent nugget and grey parts represent HAZ. For IF mode, fracture initiated at the interfacial edge and propagated through the nugget, as shown in Figure 9a. During the tensile shear test, stresses were tensile at position α and compression at position β. The nugget would rotate to
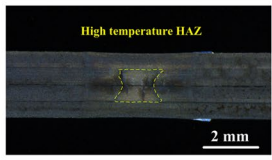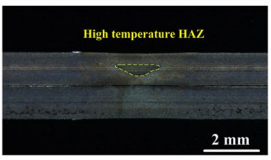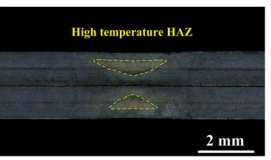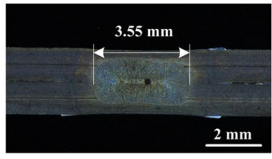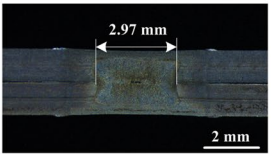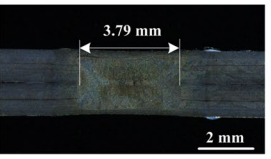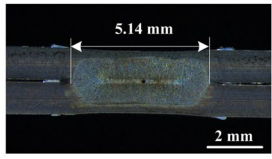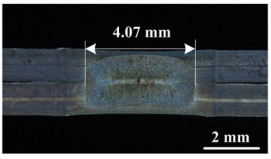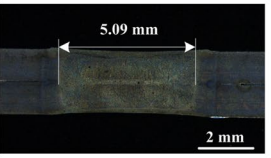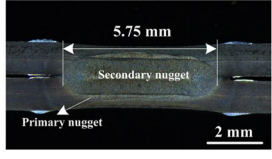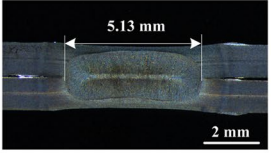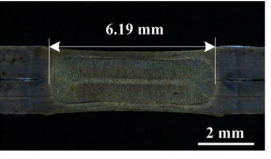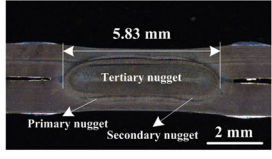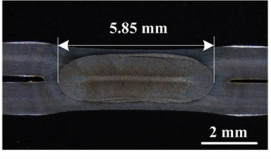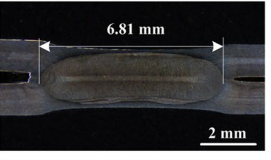
Ling *et al. Chinese Journal of Mechanical Engineering*   (2022) 35:96

Page 9 of 14

Figure 7 Nugget formation process under 7 kA without cover sheets and 7 kA and 8 kA with 0.2 mm cover sheets

align with the loading direction, and the rotation angle increased with increasing the loading. In the beginning, the rotation angle was small and the majority of the tensile load F transferred to the shear load FI along the interface. When the nugget size was small, the nugget couldn't bear the shear load and the shear fracture happened along the path A, resulting in IF mode. Shear load played the main role for IF mode. When the nugget diameter was large, the nugget could bear the shear load FI. With the increase of the tensile load and rotation angle, fracture happened along path B1 at under tensile load F, and along path B2 under the shear load along the thickness direction FT, the direction of the fracture path changed with the further rotation of the nugget. Finally, the nugget was pulled out from the lower sheet and PF mode occurred. For TF mode, fracture path C1 was similar to the fracture path B1. However, on the other side, fracture changed its position. In

fact, a crack caused by FT initiated at the edge of the nugget, as shown in Figure 9i, but as the relatively low hardness increased the fracture toughness of the nugget, the crack was arrested. After that, the final fracture happened along path C2. The initiation site at path C2 was the junction of ICHAZ and base metal, i.e., the softening zone, as shown in Figure 9h. As hardness here is the lowest, necking occurred. The driving force of fracture path C2 was also the tensile load F. As the fracture happened at different sheets, the fracture path would not encounter and TF mode occurred.

The difference of fracture location for PF and TF mode can also explain the discordance of critical nugget diameter for 0.2 mm and 0.3 mm cover sheet, as shown in Figure 4. According to Pouranvari [26], the critical nugget diameter for the steel RSW joint to avoid IF mode can be written as:
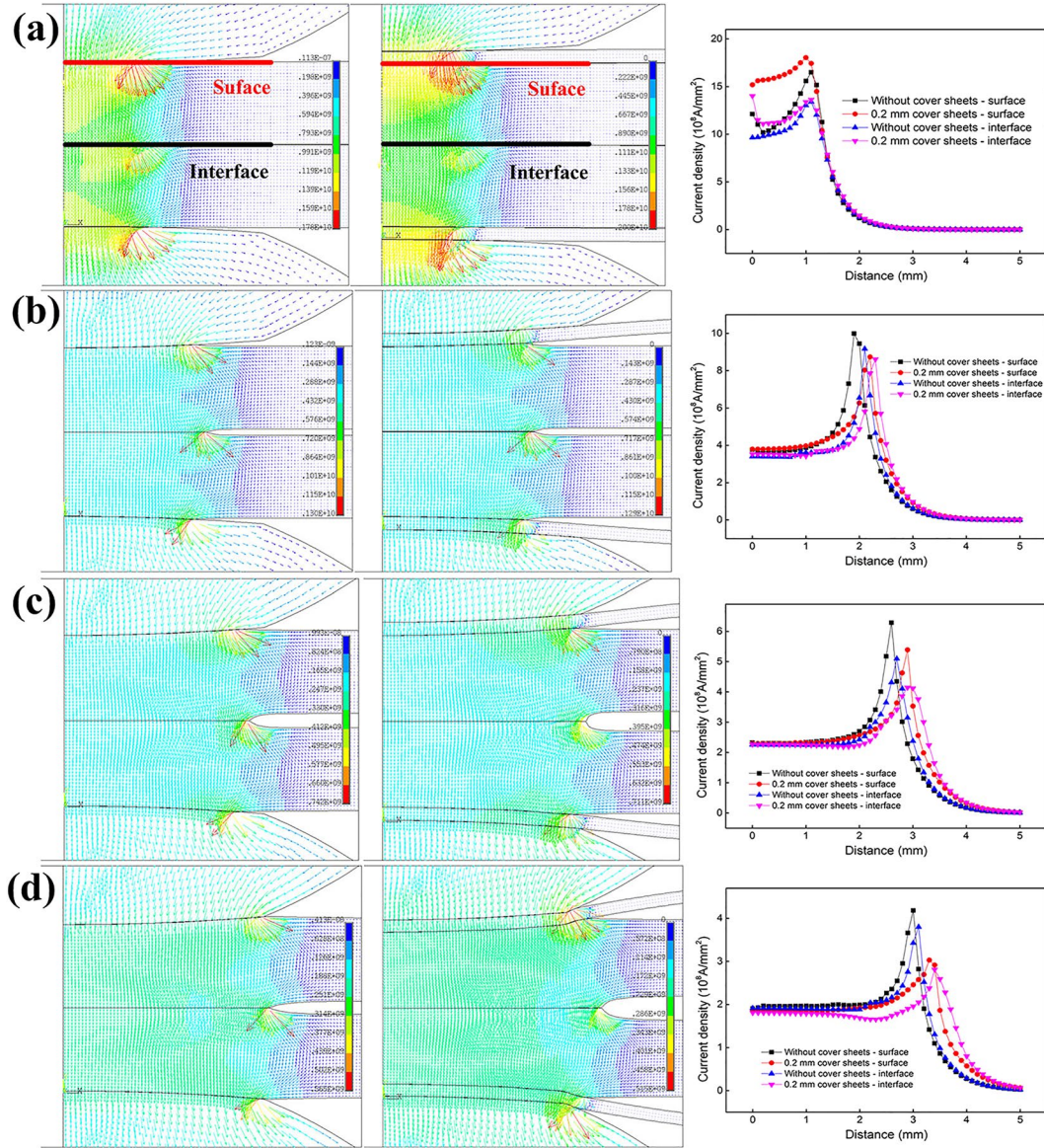
Ling *et al. Chinese Journal of Mechanical Engineering*   (2022) 35:96

Page 10 of 14

Figure 8 Calculated current density distributions and their variation at the surface and interface of the Q&P980 steel during RSW without cover sheets under 7 kA and with 0.2 mm cover sheets under 8 kA at (**a**) 1 ms, (**b**) 40 ms, (**c**) 120 ms, (**d**) 400 ms

$$d_{cr} = 4t \frac{H_{FL}}{f \times H_{FZ}}, \tag{1}$$

where d_{cr} is the critical nugget diameter, t is the thickness of the sheet, f is a material dependent constant, H_{FL} is the hardness of the pullout failure location, H_{FZ} is the hardness of the nugget. For PF mode, failure at both sides happens at the HAZ where the hardness is high, but for TF mode, failure happens at the HAZ with high hardness on one side and at the softening zone with low hardness on the other side. Base on the equation, it can

be concluded that the higher hardness of the failure location, the higher the critical nugget diameter. Thus, the critical nugget diameter of the joint with 0.3 mm cover sheets is higher than that with 0.2 mm cover sheets, as shown in Figure 4.

The fracture morphologies of different fracture modes observed by SEM are shown in Figure 11. For IF mode, as shown in Figure 11a, the red circle represents the edge of the corona bond and the yellow circle represents the edge of the nugget. Some secondary cracks can be seen outside the red dotted circle, as shown in Figure 11e.
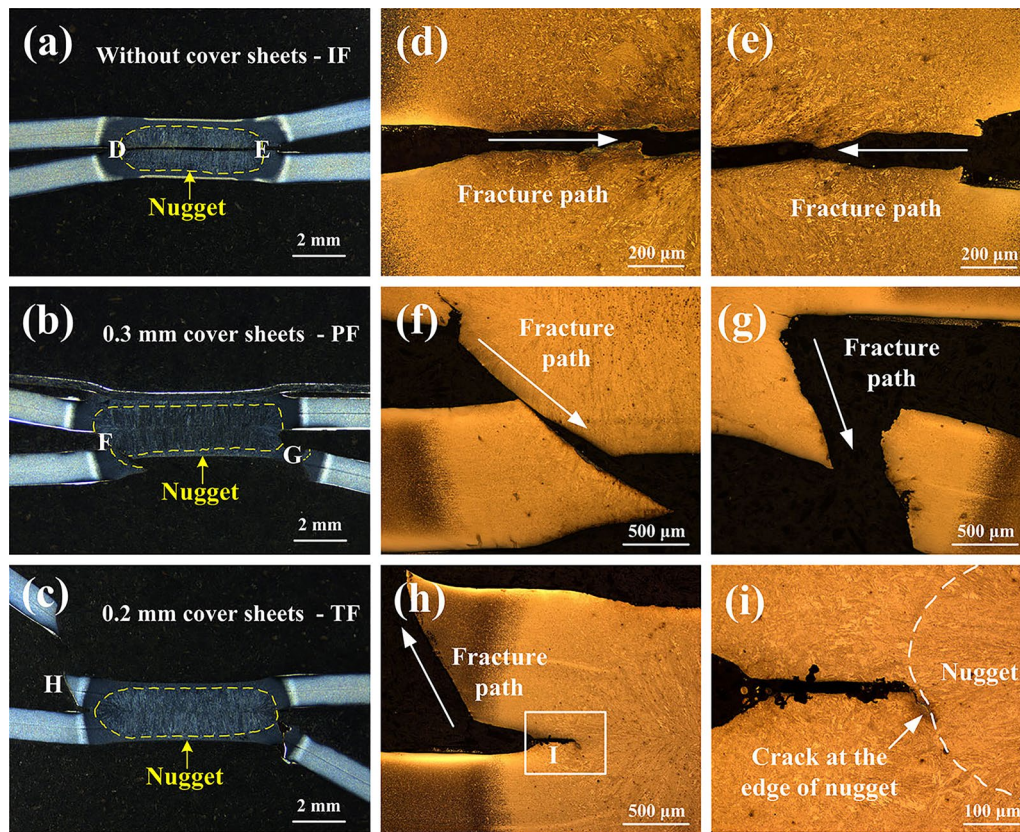
Figure 9 Profiles of fractured joints for (**a**) IF mode, (**b**) PF mode, (**c**) TF mode and (**d**–**i**) magnifications of region D–I
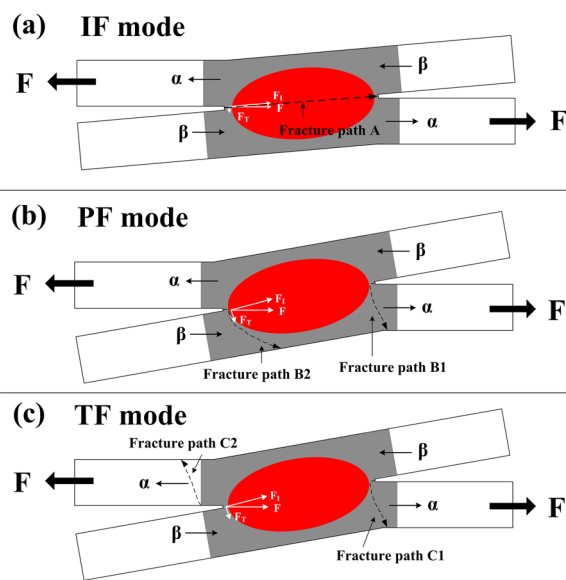

Figure 10 Schematics of failure mechanisms for (**a**) IF mode, (**b**) PF mode and (**c**) TF mode

The cracks located at the ejected soft zinc coating and they were opened by the tensile stress. Fracture firstly happened in the area between the red and yellow dotted circles, which corresponds to the lack of bonding at corona bond as shown in Figure 2e. As brittle Zn-Fe reaction products formed here, the fracture surface shows a flat cleavage characteristic (Figure 11f). Conversely, the fracture surface in the nugget area is composed of elongated dimples, as shown in Figure 11h. These dimples were formed under the shear strength at the interface, as discussed before. EDS mapping result of Zn in Figure 11b shows that the nugget area contains Zn and the residual Zn derives from the original zinc coating, which was not fully ejected during welding. Magnification of this area reveals many white substances near the dimples, which are rich in Zn. It is no doubt that the residual zinc reduces the effective bonding area of the joints. Based on the fact that we obtained larger tensile strength and PF mode on the RSW joints of uncoated Q&P980 steel with the same thickness (results are not shown here), it can be concluded that by weakening the corona bond and leaving residual Zn at the bonding area, the zinc coating deteriorates the performance of the RSW joints of
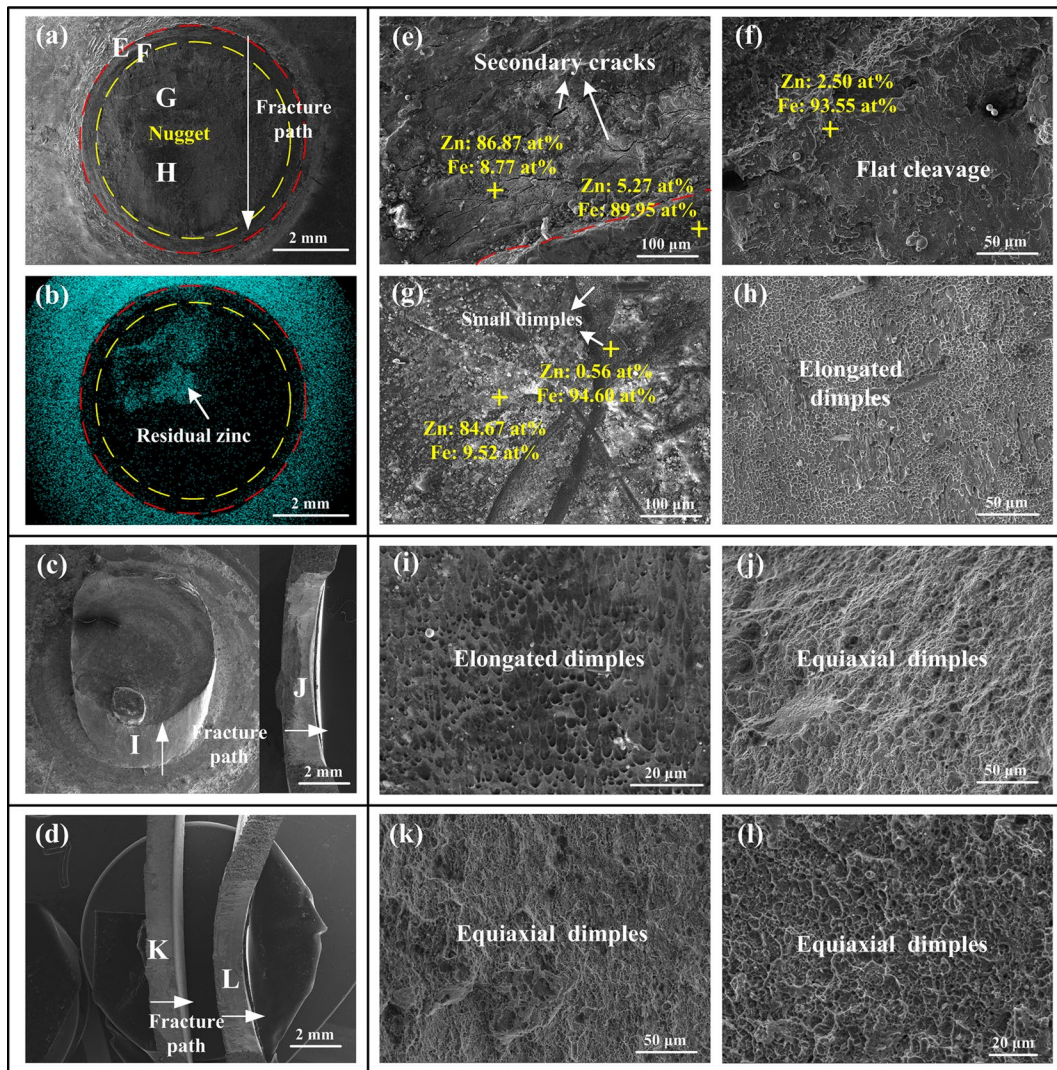
Ling *et al. Chinese Journal of Mechanical Engineering*   (2022) 35:96

Page 12 of 14

Figure 11 SEM images of fracture surface of (**a**) IF mode, (**b**) EDS zinc distribution at the surface of the IF sample, (**c**) PF mode, (**d**) TF mode and (**e–l**) magnifications of position E–L

Q&P980 steel and further promotes IF mode. For PF and TF mode, position I, which corresponds to the position E in Figure 9, consists of elongated dimples, and it further confirms that the driving force of the fracture here is shear strength. Position J, K and L, which corresponds to the position F, H and J in Figure 9, consist of equiaxial dimples, and it confirms that the driving forces of the fracture at these places are the tensile strength.

4 Conclusions

The 1.2 mm-thick Q&P980 steels were resistance spot welded with and without double-sided SPCC mild steel cover sheets. The microstructures, mechanical performances, nugget growth, and fracture behaviors of RSW joints were studied and compared. The main findings of this work can be summarized as follows:

(1) The RSW joint of Q&P980 steel included nugget, CGHAZ, FGHAZ and ICHAZ resulting from the different thermal cycles at different positions during welding. The main microstructural difference was that the surface of the Q&P980 steel was composed of martensite with cover sheets while composed of martensite and ferrite without cover sheets.

(2) The cover sheets helped postpone the expulsion and RSW could be carried out under higher welding current. The 0.2 mm cover sheets would not be welded to the base metal. By using the 0.2 mm

cover sheets, the achievable nugget diameter, nugget penetration depth, tensile shear strength and energy absorption increased by 18.5%, 13.8%, 26.9% and 52.6%, respectively. The hardness of nugget and HAZ with cover sheets decreased owing to the lower cooling rate.

(3) The nugget kept growing during the entire welding time with cover sheets, while it grew fast at the beginning of welding but gradually remained stable without cover sheets. The cover sheets helped increase the contact area and reduce the current density, and a larger area could be evenly heated, which postponed the expulsion.

(4) The larger nugget size obtained by using the cover sheets prompted the transition of fracture mode from IF mode to TF or PF mode. The fracture surface was mainly composed of elongated or equiaxial dimples, which was dependent on the stress state.

Authors' Information
Zhanxiang Ling, born in 1992, is currently a PhD candidate at *Shanghai Key Laboratory of Materials Laser Processing and Modification, Shanghai Jiao Tong University, China.* He received his bachelor and master degree from *Tianjin University, China*, in 2014 and 2017, respectively. His research interests include resistance spot welding of high-strength steels and light-weight metals.
Ting Chen, born in 1994, is currently an PhD candidate. He received his bachelor and master degree from *Shanghai Jiao Tong University, China*, in 2017 and 2020, respectively.
Liang Kong, born in 1966, is currently an associate research fellow at *Shanghai Jiao Tong University, China*.
Ming Wang, born in 1960, is currently a professor at *Shanghai Jiao Tong University, China*.

References
[1] M Pouranvari, S P H Marashi. Critical review of automotive steels spot welding: process, structure and properties. *Science & Technology of Welding & Joining*, 2013, 18(5): 361-403.

[2] C W Ji, I Jo, H Lee, et al. Effects of surface coating on weld growth of resistance spot-welded hot-stamped boron steels. *Journal of Mechanical Science & Technology*, 2014, 28(11): 4761-4769.

[3] M Tumuluru. Some considerations in the resistance spot welding of dual phase steels. *The 5th International Seminar on Advances in Resistance Welding*, Toronto, Canada, 2018: 50-65.

[4] D W Zhao, Y X Wang, L Zhang, et al. Effects of electrode force on microstructure and mechanical behavior of the resistance spot welded DP600 joint. *Materials & Design*, 2013, 50: 72-77.

[5] L Cretteur, A I Koruk, L Tosal-Martínez. Improvement of weldability of TRIP steels by use of in-situ pre-and post-heat treatments. *Steel Research*, 2002, 73(6-7): 314-319.

[6] M Pouranvari. Understanding the factors controlling the interfacial failure strength of advanced high-strength steel resistance spot welds: hardness vs. fracture toughness. *Science & Technology of Welding & Joining*, 2018, 23(6): 520-526.

[7] A Chabok, E Van der Aa, J T M De Hosson, et al. Mechanical behavior and failure mechanism of resistance spot welded DP1000 dual phase steel. *Materials & Design*, 2017, 124: 171-182.

[8] P Eftekharimilani, E M van der Aa, M J M Hermans, et al. Microstructural characterisation of double pulse resistance spot welded advanced high strength steel. *Science & Technology of Welding & Joining*, 2017, 22(7): 545-554.

[9] X D Liu, Y B Xu, R D K Misra, et al. Mechanical properties in double pulse resistance spot welding of Q&P 980 steel. *Journal of Materials Processing Technology*, 2019, 263: 186-197.

[10] R Chen, M Lou, Y Li, et al. Improving weldability of Al-Si coated press hardened steel using stepped current pulse schedule. *Journal of Manufacturing Processes*, 2019, 48: 31-43.

[11] J Yu, D Choi, S Rhee. Improvement of weldability of 1 GPa grade twin-induced plasticity steel. *Welding Journal*, 2014, 93(3): 78-84.

[12] Y B Li, Q Shen, Z Lin, et al. Quality improvement in resistance spot weld of advanced high strength steel using external magnetic field. *Science & Technology of Welding & Joining*, 2011, 16(5): 465-469.

[13] H Aghajani, M Pouranvari. A pathway to produce strong and tough martensitic stainless steels resistance spot welds. *Science & Technology of Welding & Joining*, 2019, 24(3): 185-192.

[14] S Satonaka, C Iwamoto, G I Murakami, et al. Resistance spot welding of magnesium alloy sheets with cover sheets. *Welding in the World*, 2012, 56(7-8): 44-50.

[15] R Qiu, C Iwamoto, S Satonaka. Interfacial microstructure and strength of steel/aluminum alloy joints welded by resistance spot welding with cover sheet. *Journal of Materials Processing Technology*, 2009, 209(8): 4186-4193.

[16] J Yu. Effect of cover sheet on dissimilar three-steel sheets resistance spot welding. *The International Journal of Advanced Manufacturing Technology*, 2017, 89(1-4): 483-491.

[17] M Pouranvari, S Sobhani, F Goodarzi. Resistance spot welding of MS1200 martensitic advanced high strength steel: Microstructure-properties relationship. *Journal of Manufacturing Processes*, 2018, 31: 867-874.

[18] Z Wan, H P Wang, M Wang, et al. Numerical simulation of resistance spot welding of Al to zinc-coated steel with improved representation of contact interactions. *International Journal of Heat & Mass Transfer*, 2016, 101: 749-763.

[19] Y Zhou, S J Dong, K J Ely. Weldability of thin sheet metals by small-scale resistance spot welding using high-frequency inverter and capacitor-discharge power supplies. *Journal of Electronic Materials*, 2001, 30(8): 1012-1020.

[20] M Pouranvari, S P H Marashi. Failure of resistance spot welds: Tensile shear versus coach peel loading conditions. *Ironmaking & Steelmaking*, 2012, 39(2): 104-111.

[21] M Alizadeh-Sh, S P H Marashi, M Pouranvari. Resistance spot welding of aisi 430 ferritic stainless steel: phase transformations and mechanical properties. *Materials & Design*, 2014, 56: 258-263.

[22] M Pouranvari, A Abedi, P Marashi, et al. Effect of expulsion on peak load and energy absorption of low carbon steel resistance spot welds. *Science & Technology of Welding & Joining*, 2008, 13(1): 39-43.

[23] M Tamizi, M Pouranvari, M Movahedi. Welding metallurgy of martensitic advanced high strength steels during resistance spot welding. *Science & Technology of Welding & Joining*, 2016, 22(4): 327-335.

[24] P R Spena, M D Maddis, F Lombardi, et al. Dissimilar resistance spot welding of Q&P and TWIP steel sheets. *Advanced Manufacturing Processes*, 2016, 31(3): 291-299.

[25] K Sirin, S Y Sirin, E Kaluc. Influence of the interpass temperature on t8/5 and the mechanical properties of submerged arc welded pipe. *Journal of Materials Processing Technology*, 2016, 238: 152-159.

[26] M Pouranvari. Analysis of fracture mode of galvanized low carbon steel resistance spot welds. *International Journal of Multidisciplinary Sciences and Engineering*, 2011, 2(6): 36-40.